Short Papers

Equidistant Fish-Eye Calibration and Rectification by Vanishing Point Extraction

Ciarán Hughes, *Member*, *IEEE*,
Patrick Denny, *Member*, *IEEE*,
Martin Glavin, *Member*, *IEEE*, and
Edward Jones, *Member*, *IEEE*

Abstract—In this paper, we describe a method to photogrammetrically estimate the intrinsic and extrinsic parameters of fish-eye cameras using the properties of equidistance perspective, particularly vanishing point estimation, with the aim of providing a rectified image for scene viewing applications. The estimated intrinsic parameters are the optical center and the fish-eye lensing parameter, and the extrinsic parameters are the rotations about the world axes relative to the checkerboard calibration diagram.

Index Terms—Fish-eye, calibration, perspective.

1 Introduction

THE spherical mapping of most fish-eye lenses used in machine vision introduces symmetric radial displacement of points from the ideal rectilinear points in an image around an optical center. The visual effect of this displacement in fish-eye optics is that the image will have a higher resolution in the central areas, with the resolution decreasing nonlinearly toward the peripheral areas of the image.

Fish-eye cameras manufactured to follow the equidistance mapping function are designed such that the distance between a projected point and the optical center of the image is proportional to the incident angle of the projected ray, scaled only by the equidistance parameter f, as described by the projection equation [1], [2]:

$$r_d = f\theta, \tag{1}$$

where r_d is the fish-eye radial distance of a projected point from the center, and θ is the incident angle of a ray from the 3D point being projected to the image plane. This is one of the more common mapping functions that fish-eye cameras are designed to follow, the others being the *stereographic*, *equisolid*, and *orthogonal* mapping functions.

In the projection of a set of parallel lines to the image plane using the rectilinear pinhole perspective model, straight lines will be imaged as straight lines and parallel sets of straight lines converge at a single vanishing point on the image plane. However, in equidistance projection perspective, the projection of a parallel set of lines in worlds system will be a set of curves that converge at two vanishing points, and the line that intersects the two vanishing points also intersects the optical center of the camera. This property was demonstrated explicitly in our earlier work [3]. In that work, it was also demonstrated how the vanishing points could be used to estimate the optical center of the fish-eye camera, and it was shown that circles provided an accurate approximation of the projection of a straight line to the equidistance image plane.

Hartley and Kang [4] provide one of the more recently proposed parameter-free methods of calibrating cameras and compensating for distortion in all types of lenses, from standard low-distortion lenses through high distortion fish-eye lenses. Other important works on fish-eye calibration include [5], [6]. While there has been some work done in the area of camera perspective with a view to calibration, there has been little work specifically on wide-angle camera perspective. Early work on calibration via perspective properties included [7], where a hexagonal calibration image was used to extract three co-planar vanishing points and thus to extract the camera parameters. Other work on the calibration of cameras using perspective principles and vanishing points has been done in, for example, [8], [9], [10], [11]. However, none of these publications address fish-eye cameras with strong optical displacement, i.e., these calibration methods assume that the cameras follow the pinhole projection mapping function.

In this paper, we demonstrate how equidistance vanishing points can be used to estimate a camera's intrinsic fish-eye parameters (both the optical center and the equidistance parameter f) and extrinsic orientation parameters (orientation about the world axes), using a standard checkerboard test diagram. Additionally, we compare the accuracy of using circle fitting (as proposed in [3]) and the more general conic fitting.

In Section 2, we show how the vanishing points can be extracted from a single full-frame image of a checkerboard diagram under equidistance projection. To extract the vanishing points, the mapped lines of the test diagram are fitted with both circles and the general conic section equation. While the fitting of circles is a simpler solution to the calibration problem, we show that the fitting of the general conic equation to the mapped lines is the more accurate solution. In Section 3, we show how intrinsic and extrinsic camera parameters can be estimated using the extracted vanishing points, and in Section 4, we test and compare the accuracy of the proposed methods using a large set of synthetically created images, and a smaller set of real images.

2 Determining the Vanishing Point Locations

In this section, we will describe how the vanishing points can be extracted from a full-frame equidistance projected wide-angle image of a traditional checkerboard test diagram, such as that shown in Fig. 1. The checkerboard diagram consists of two sets of parallel lines, each with a corresponding pair of vanishing points. We will denote the fish-eye vanishing point pair corresponding to the approximately horizontal direction as $\mathbf{w}_{X,1}$ and $\mathbf{w}_{X,2}$, as this is the world axis system that these vanishing points are related to. Similarly, we denote the vertical vanishing point pair as $\mathbf{w}_{Y,1}$ and $\mathbf{w}_{Y,2}$. If the fish-eye vanishing points $\mathbf{w}_{X,1}$, $\mathbf{w}_{X,2}$, $\mathbf{w}_{Y,1}$, and $\mathbf{w}_{Y,2}$ are known, given the optical center and equidistance parameter f, the corresponding rectilinear vanishing points $\mathbf{v}_X$ and $\mathbf{v}_Y$ can simply be determined by undistorting $\mathbf{w}_{X,1}$ and $\mathbf{w}_{Y,1}$, or $\mathbf{w}_{X,2}$ and $\mathbf{w}_{Y,2}$.

2.1 Using Circles

Here, we describe a method of extracting the vanishing points by fitting circles to the equidistance projection of checkerboard lines. Strand and Hayman [12], Barreto and Daniilidis [13], and Bräuer-Burchardt and Voss [14] suggest that the projection of straight lines in cameras exhibiting radial distortion results in circles on the

- *C. Hughes and P. Denny are with the Vision Technology and Expertise Group, Valeo Vision Systems, Tuam, Co. Galway, Ireland. E-mail: {ciaran.hughes, patrick.denny}@valeo.com.*
- *M. Glavin and E. Jones are with Electrical and Electronic Engineering, College of Engineering and Informatics, National University of Ireland, Galway, Ireland. E-mail: {martin.glavin, edward.jones}@nuigalway.ie.*

Manuscript received 3 Apr. 2009; revised 1 Apr. 2010; accepted 5 July 2010; published online 19 Aug. 2010.
Recommended for acceptance by A. Fitzgibbon.
For information on obtaining reprints of this article, please send e-mail to: tpami@computer.org, and reference IEEECS Log Number TPAMI-2009-04-0208.
Digital Object Identifier no. 10.1109/TPAMI.2010.159.

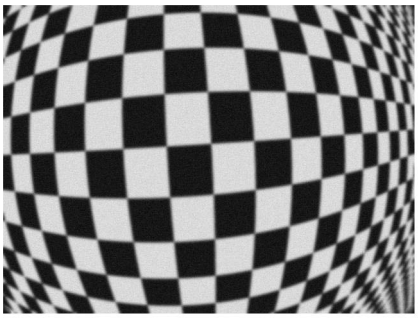

Fig. 1. Fish-eye checkerboard test diagram.

image plane. Bräuer-Burchardt and Voss, in contrast to the others, explicitly use fish-eye images in their examples. All three methods assume that the camera system follows the *division model*. However, in our previous work [3], we demonstrated that the equidistance projection of straight lines can also be modeled as circles.

2.1.1 Extracting the Vanishing Points

The first step to extract the vanishing points from a fish-eye image of the checkerboard test diagram is to separate the curves into their vertical and horizontal sets. Here, for example, we used an optimized Sobel edge detector [15] to extract the edges. The gradient information from the edge detection was used to separate the edges into their horizontal and vertical sets. Discontinuities in lines caused by corners in the grid are detected using a suitable corner detection method (for example, [16]), and thus corrected. Fig. 2 shows edges extracted from the checkerboard test image in Fig. 1.

Schaffalitzky and Zisserman [17] describe how the vanishing point for a non-fish-eye set of rectilinear projected concurrent lines can be estimated, using the Maximum Likelihood Estimate (MLE), to provide a set of corrected lines that are exactly concurrent. The method described can be easily extended to support arcs of circles, and two vanishing points, rather than lines and single vanishing points. This is described in detail in [3]. Fig. 3 shows the two sets of fitted circles with the MLE-determined vanishing points.

2.2 Using Conics

It is proposed that any error in using circle fitting can be reduced by allowing a fit to a more general conic equation. This gives the fit greater degrees of freedom and therefore greater potential for accuracy. A conic on the image plane can be described as:

$$Au^2 + 2Buv + Cv^2 + 2Du + 2Ev + F = 0. \tag{2}$$

Zhang [18] describes several methods of fitting conics to image data. Barreto and Araujo [19] also describe in detail methods of fitting conics to projected lines, though in that case the fitting is for paracatadioptric projections (i.e., projections involving a camera that consists of lens and mirror arrangements), rather than equidistance projections. In this case, we use a method similar to

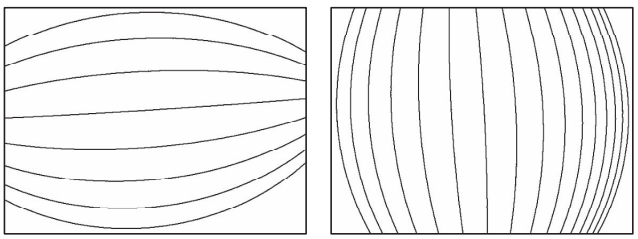

(a) (b)

Fig. 2. Extracted edges for use in calibration. (a) Vertical edges and (b) horizontal edges.

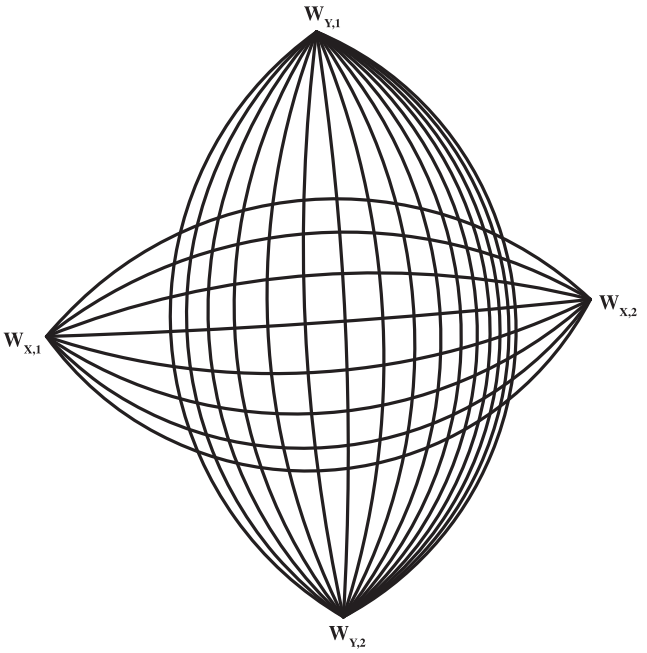

Fig. 3. The two sets of circles, convergent with the four vanishing points, that correspond to the checkerboard diagram in Fig. 1.

that of using circles, i.e., the edges are extracted in the same manner and the MLE extraction of the vanishing point is used. However, instead of using a least-mean-squares (LMS) algorithm to fit circles, we use a similar algorithm to fit the general equation of a conic (which has five degrees of freedom, compared to the three degrees of freedom that the equation of a circle has). Other than using conic fitting, the optimization and other steps are the same as for the circle fit.

3 Determining the Camera Parameters

We now describe how, having estimated the locations of the vanishing points (by either circle or conic fitting), the intrinsic fish-eye parameters and the orientation parameters of the camera can be extracted. In Section 4, we examine the accuracy of using circle and conic fitting to determine the parameters.

The vanishing points in equidistance projection, $\mathbf{w}_1$ and $\mathbf{w}_2$, are given by [3]:

$$\mathbf{w}_1 = \begin{cases} \begin{bmatrix} D_x \\ D_y \end{bmatrix} \frac{f}{\sqrt{D_x^2+D_y^2}} E, & \phi_{\text{vp}} g e 0, \\ \begin{bmatrix} D_x \\ D_y \end{bmatrix} \frac{f}{\sqrt{D_x^2+D_y^2}} (-E), & \phi_{\text{vp}} < 0, \end{cases} \tag{3}$$

$$\mathbf{w}_2 = \begin{cases} \begin{bmatrix} D_x \\ D_y \end{bmatrix} \frac{f}{\sqrt{D_x^2+D_y^2}} (E-\pi), & \phi_{\text{vp}} \geq 0, \\ \begin{bmatrix} lD_x \\ D_y \end{bmatrix} \frac{f}{\sqrt{D_x^2+D_y^2}} (\pi-E), & \phi_{\text{vp}} < 0, \end{cases} \tag{4}$$

where

$$E = \arctan\left(\frac{\sqrt{D_x^2+D_y^2}}{D_z}\right), \tag{5}$$

where $\mathbf{D} = [D_x, D_y, D_z]$ is the vector that describes the direction of the parallel lines in the scene and ϕ_{vp} is the angle the line that intersects the vanishing point and the optical center makes with the u-axis of the image plane ($-\frac{\pi}{2} < \phi_{\text{vp}} \leq \frac{\pi}{2}$).

In our prior work [3], it was demonstrated that the line that joins the two vanishing points (the horizon line) also intersects the

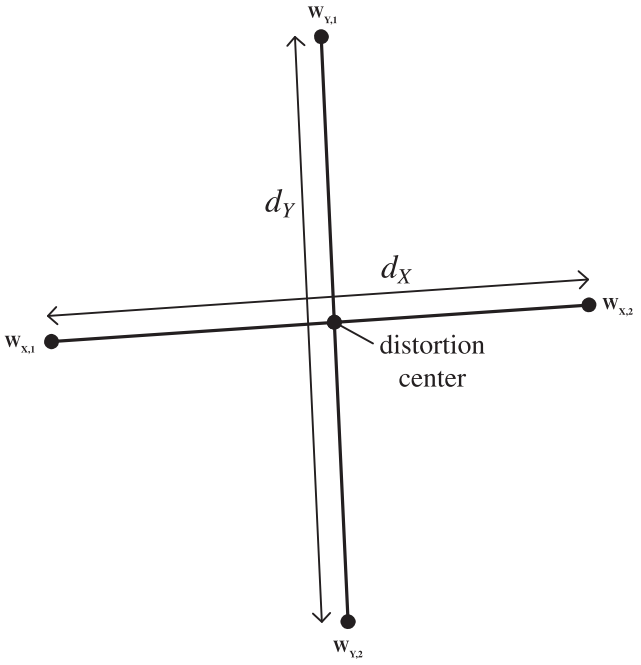

Fig. 4. Estimating the optical center and the equidistance parameter f.

optical center. From the previous section, two pairs of vanishing points (with their two corresponding horizon lines) can be estimated from a fish-eye image of a checkerboard test diagram. The intersection of these two horizon lines is, therefore, an estimate of the optical center (Fig. 4).

To estimate f, we examine the distance between the vanishing points described by (3) and (4), which is:

$$|\mathbf{w_1}-\mathbf{w_2}| = \sqrt{\left(w_{1,u}-w_{2,u}\right)^2+\left(w_{1,v}-w_{2,v}\right)^2}. \tag{6}$$

It is straightforward to show that this reduces to:

$$\begin{aligned}|\mathbf{w_1}-\mathbf{w_2}| &= \sqrt{\frac{\pi^2}{D_X^2+D_Y^2}f^2D_X^2+\frac{\pi^2}{D_X^2+D_Y^2}f^2D_Y^2} \\ &= \sqrt{\pi^2f^2} = f\pi.\end{aligned} \tag{7}$$

Therefore, given the vanishing points, f can simply be determined as:

$$f = \frac{|\mathbf{w_1}-\mathbf{w_2}|}{\pi}. \tag{8}$$

As shown in Figs. 3 and 4, there are two distances d_X and d_Y that have corresponding equidistance parameters f_X and f_Y. The estimated value for f is simply taken as the average of f_X and f_Y.

Given the fish-eye parameters, the aim is to convert the fish-eye image to a rectilinear image. This is done by converting the points in the equidistance image plane to their equivalent points on the rectilinear (pinhole) image plane. Rectilinear projection is described as:

$$r_u = f\tan(\theta). \tag{9}$$

The function that describes the conversion of an equidistance projected point to a rectilinear projected point is obtained by combining (1) and (9):

$$r_u = f\tan\left(\frac{r_d}{f}\right), \tag{10}$$

and its inverse:

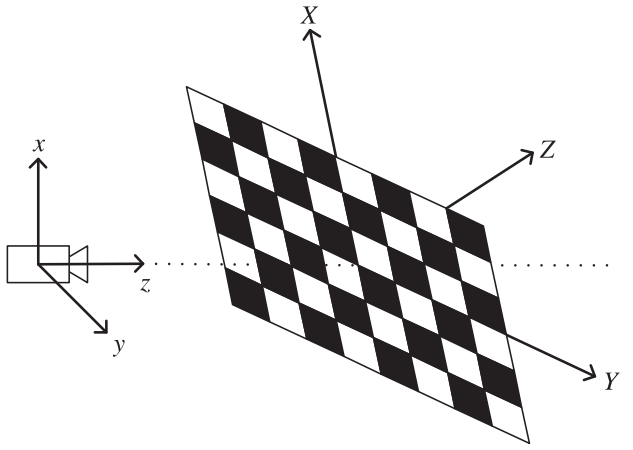

Fig. 5. Rotation of the camera/world coordinate systems.

$$r_d = f\arctan\left(\frac{r_u}{f}\right). \tag{11}$$

3.1 Camera Orientation

In previous sections, we assumed that the world coordinate system was centered on the center of projection of the camera. However, in order to take into account rotation between the camera coordinate system and the test diagram, it is more convenient for the world coordinates to be located at the test diagram, as described in Fig. 5, and rotated away from the camera coordinate systems. Extending the rectilinear pinhole camera model to include translation and rotation gives

$$\mathbf{x_u} = \mathbf{K}[\mathbf{R}|\mathbf{T}]\mathbf{X}, \tag{12}$$

where $\mathbf{R}$ is a 3×3 rotation matrix and $\mathbf{T}$ is a three element column vector, describing the translational mapping from world coordinates to camera coordinates. Gallagher [20] describes how the location of the vanishing points is independent of the translation vector $\mathbf{T}$, and is given by

$$\mathbf{V} = [\mathbf{v}_X, \mathbf{v}_Y, \mathbf{v}_Z] = \mathbf{KR}, \tag{13}$$

where $\mathbf{V}$ is the matrix of vanishing point locations, made up from the homogeneous column vectors $\mathbf{v}_X$, $\mathbf{v}_Y$, and $\mathbf{v}_Z$ that describe the vanishing points on the image plane related to each of the X, Y, and Z-axes, respectively. Under rotation about the X and Y-axes only, the vanishing points become [20]

$$\mathbf{V}_{XY} = \begin{bmatrix} f\cos\alpha & 0 & f\sin\alpha \\ f\sin\beta\sin\alpha & f\cos\alpha & -f\sin\beta\cos\alpha \\ -\cos\beta\sin\alpha & \sin\alpha & \cos\beta\cos\alpha \end{bmatrix}. \tag{14}$$

This is equivalent to first rotating about the Y-axis by angle β, and then rotating about the original X-axis by angle α. It is important to

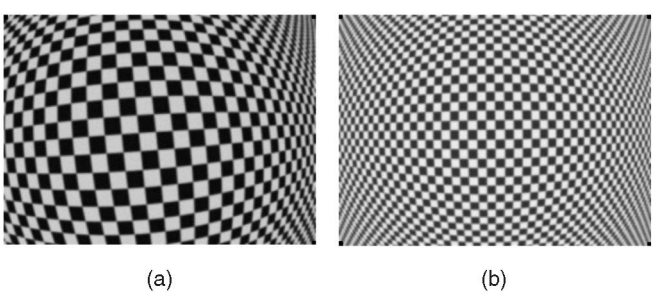

Fig. 6. Synthetic image samples.

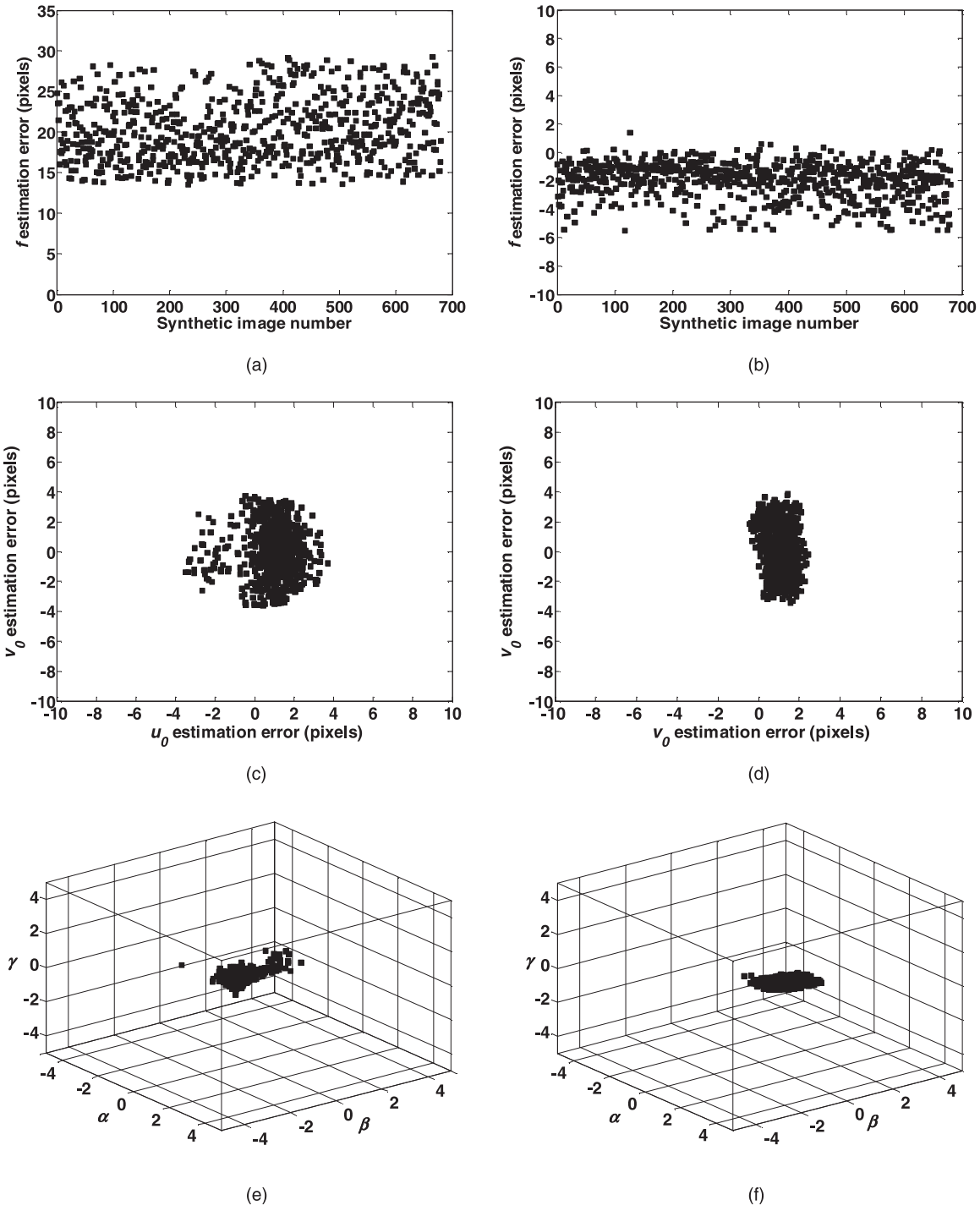

Fig. 7. Parameter estimation errors using synthetic images. (a) Distribution of the estimation errors of f using circle fitting and (b) using conic fitting. (c) Distribution of the optical center estimation errors using circle fitting and (d) using conic fitting. (e) Distribution of the camera orientation estimations using circle fitting (in degrees) and (f) using conic fitting (in degrees). The resolution for all images was 640×480.

note that after the homogeneous $\mathbf{v}_Y$ is converted to image plane coordinates, it is constrained to fall on the image plane v-axis. Adding further rotation about the Z-axis by angle γ results in

$$\mathbf{V} = \mathbf{R}_Z \mathbf{V}_{XY}, \tag{15}$$

where

$$\mathbf{R}_Z = \begin{bmatrix} \cos\gamma & -\sin\gamma & 0 \\ \sin\gamma & \cos\gamma & 0 \\ 0 & 0 & 1 \end{bmatrix}. \tag{16}$$

Thus, rotating about the Z-axis results in the vanishing points $\mathbf{V}_{XY}$ being rotated by the same angle.

The method for estimating $\mathbf{v}_X$ and $\mathbf{v}_Y$ was described in the previous section. Considering that $\mathbf{v}_Y$ is constrained to fall on the v-axis in image plane coordinates, the angle of rotation about the Z-axis can be determined by measuring the angle γ that $\mathbf{v}_Y$ makes with the v-axis at the origin [20]. Given $\mathbf{v}_X$, $\mathbf{v}_Y$, and γ, the other two orientation parameters can be determined from the first two column vectors in (15). Thus, given the three orientation parameters, the rotation matrix $\mathbf{R}$ can be constructed and used to rectify a given image.

TABLE 1
Errors of the Parameter Estimations for the Synthetic Image Set

	Circle Fitting		Conic Fitting	
	μ	σ	μ	σ
f	20.296	3.864	-2.012	1.264
c_u	0.173	1.137	0.107	0.587
c_v	1.046	1.736	0.933	1.637
α	0.365	0.459	-0.0690	0.522
β	0.785	0.363	-0.227	0.301
γ	-0.0261	0.0490	-0.0144	0.0312

The mean μ and the standard deviation σ of the errors of the camera parameter estimation using the synthetic images. f, c_u, and c_v are in pixels; α, β, and γ are in degrees.

TABLE 2
Intrinsic Fish-Eye Parameter Estimations Using Real Images

	Camera 1		Camera2		Camera3	
	μ	σ	μ	σ	μ	σ
	Circle Fitting					
f	304.06	1.871	291.42	3.138	383.69	2.379
c_u	254.81	1.101	206.59	0.564	249.91	1.365
c_v	275.56	1.537	299.92	1.837	282.29	1.593
	Conic Fitting					
f	270.56	1.134	279.82	1.237	361.01	0.643
c_u	254.93	1.055	207.99	0.568	251.46	0.904
c_v	275.65	1.362	298.78	1.495	283.79	1.128

The mean μ and the standard deviation σ of the errors of the camera parameter estimations of the three cameras (15 images per camera) used in the experiments. All values are in pixels. Camera 1 is a 170° field-of-view equidistance fish-eye camera, Camera 2 has a 163° field-of-view, Camera 3 has a 103° field-of-view.

4 Results

4.1 Synthetic Images

To determine the accuracy of the parameter estimation, the algorithm was run on a set of synthetic images. The synthetic images were created with a set of known parameters, and a number of imperfections were added (sharpness, noise, and imperfect illumination). The method used to create the synthetic images is the same as that described in [3].

Fig. 6 shows two of the synthetically created calibration images. A total of 680 synthetic images were created, and the equidistance parameter, optical center, and orientations were estimated using both circle fitting and conic fitting. Fig. 7 shows the distributions of the errors of the parameter estimates for the synthetic images, and Table 1 shows the mean and standard deviations of the errors. The errors are calculated as the difference of the estimated parameters and the modeled parameters. It can be seen from both Fig. 7 and Table 1 that, in general, both the average error and the deviation are smaller for the conic fitting method than the circle fit method. This is particularly true for the error in the estimation of f for the

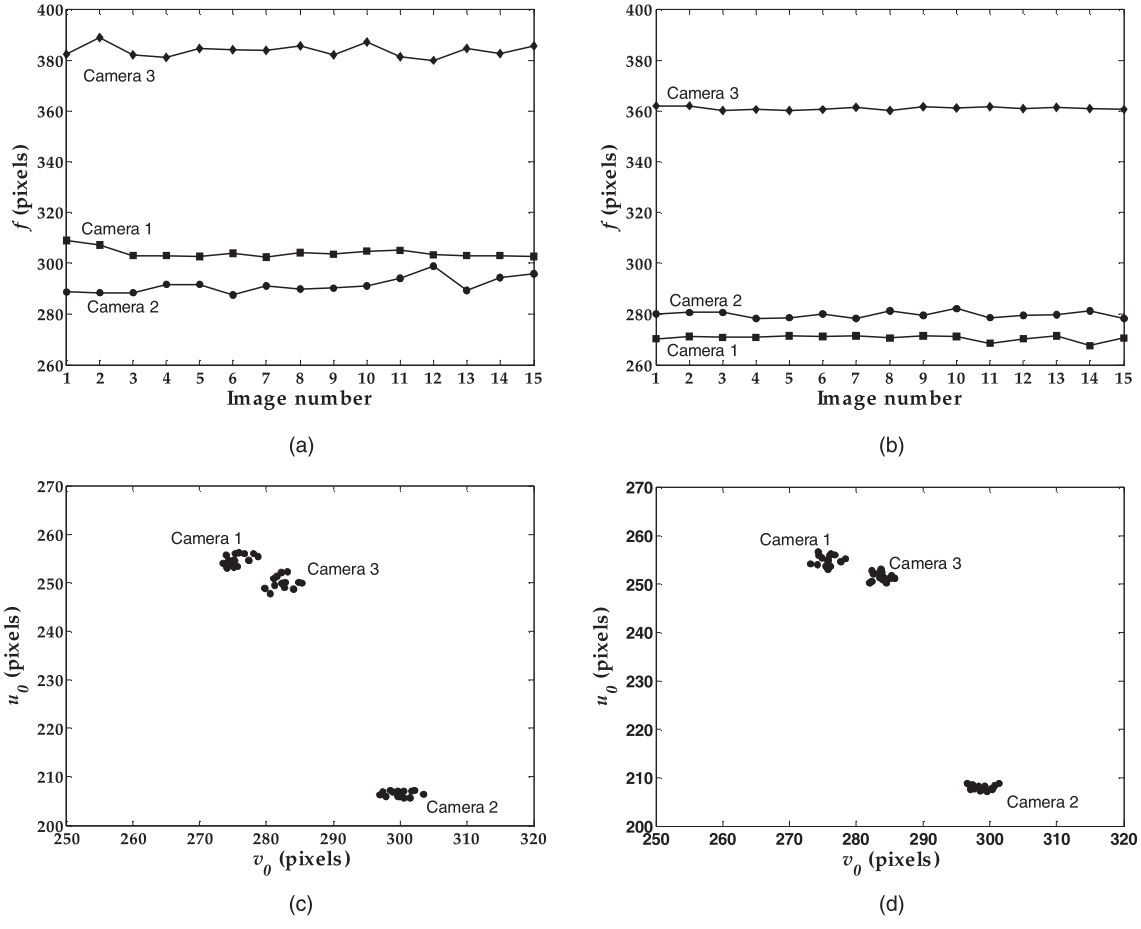

Fig. 8. Parameter estimation errors from real images taken from three cameras (15 images per camera). (a) Estimation of f using the circle fitting method for each image from each camera, (b) using the conic fitting method, (c) distributions of the optical center estimation using the circle fitting method, (d) using the conic fitting method. Camera 1 is a 170-degree field-of-view equidistance fish-eye camera, Camera 2 has a 163-degree field-of-view, Camera 3 is a moderate wide-angle camera with a 103-degree field-of-view. The sample resolution of all images was 640×480 pixels.

TABLE 3
Extrinsic Orientation Parameter Estimations Using Real Images

Im. #	Circle Fitting			Conic Fitting		
	α	β	γ	α	β	γ
1	-7.051	-13.136	6.495	-6.864	-13.471	6.471
2	-4.122	-15.556	-2.008	-3.820	-15.849	-2.318
3	-0.699	1.225	-0.562	-0.827	0.989	-0.585
4	-8.498	1.940	-0.385	-8.502	2.330	-0.553
5	-3.929	0.711	-0.494	-3.601	0.269	-0.130
6	-0.904	1.531	-0.561	-0.825	1.792	-0.470
7	-5.162	0.081	-0.518	-5.122	-0.377	-0.267
8	3.414	8.936	0.622	3.481	8.688	0.620
9	1.682	2.706	2.024	1.916	2.938	2.471
10	-14.054	5.858	-0.581	-14.204	5.638	-0.315
11	-6.106	6.132	-7.755	-6.341	6.399	-7.580
12	-9.309	6.898	-6.411	-9.114	6.993	-6.085
13	-13.678	-3.680	0.411	-14.057	-3.860	0.909
14	-3.924	-3.825	0.414	-4.254	-3.396	0.588
15	-5.749	-0.621	0.127	-5.943	-0.854	-0.180

The estimated orientation parameters for the 15 calibration images of Camera 1. All values are in degrees. Similar results were obtained for Cameras 2 and 3.

circle fitting method, which is considerably higher than for the conic fitting method (Table 1).

The error in estimating c_v is larger than that for c_u for both the circle and conic fitting methods. This can be explained by the fact that the estimation of c_u is primarily determined by the horizontal horizon line. An error in the estimation of the vertical horizon line will have less of an impact on the estimation of c_u than an error in the estimation of the horizontal horizon line. The opposite is true for the estimation of c_v. Considering that the horizontal curves imaged in, for example, Fig. 6 have more data points (640 data points as opposed to 480), it is reasonable to assume that the circle/conic fitting to these imaged curves will be more accurate than to the vertical curves. Therefore, the estimation of the horizontal horizon line will be more accurate than the vertical, and thus the estimation of c_u tends to be more accurate than c_v.

4.2 Real Images

In this section, we examine the accuracy of the calibration algorithms using real images of the checkerboard calibration diagram captured using three different wide-angle cameras. For each camera, 15 images were captured and processed using the parameter estimation algorithms.

Fig. 8 shows the results from the parameter estimations for each image from each camera. The results, in general, back up the synthetic image results. The estimation of f, using circle fitting, returns a higher value for f than the conic fitting method. While

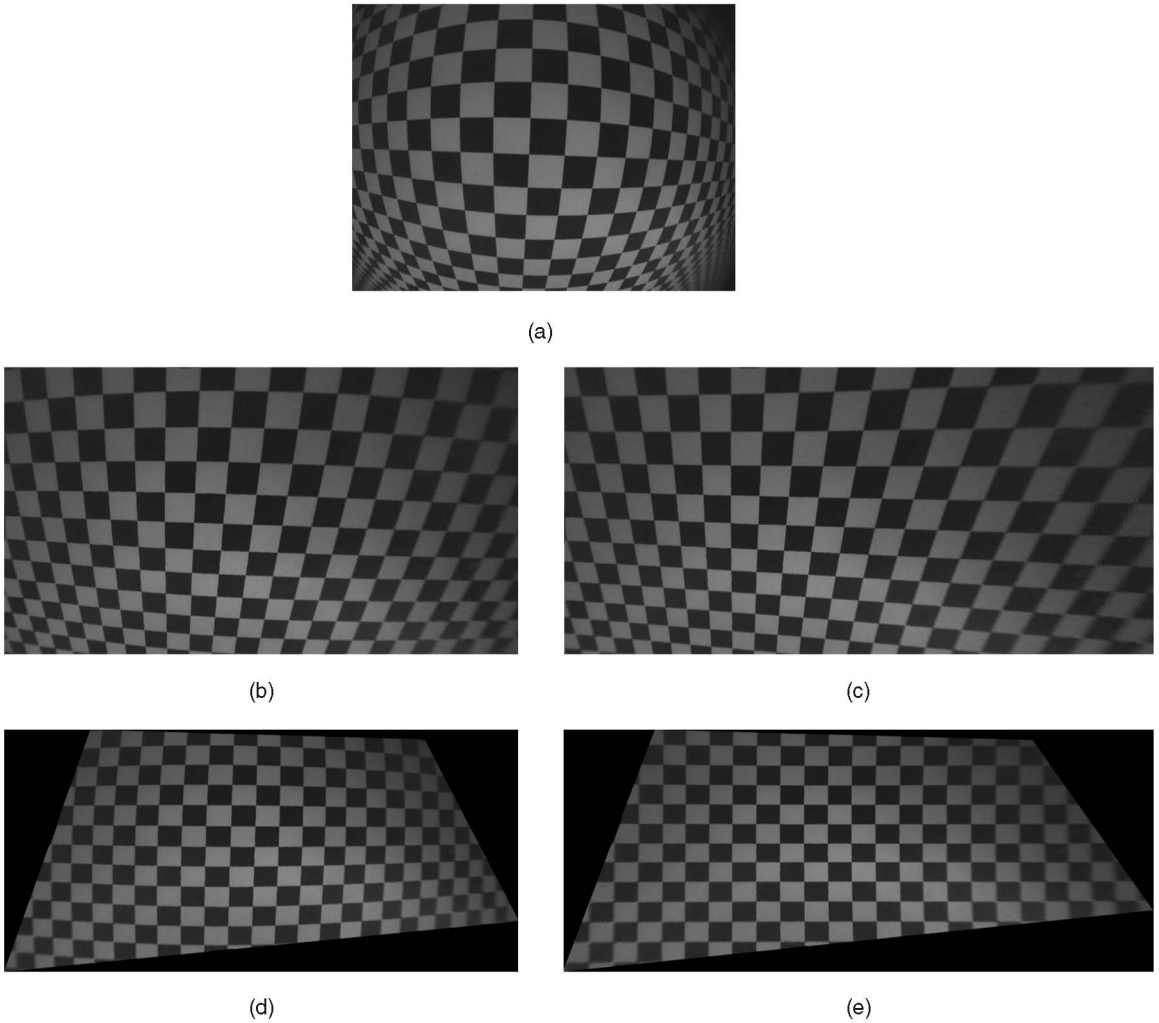

Fig. 9. Rectification of a checkerboard image from Camera 3. (a) Original image, (b) calibrated using circle fit parameters, (c) using conic fit parameters, (d) rectification using circle fit parameters, and (e) rectification using conic fit parameters.

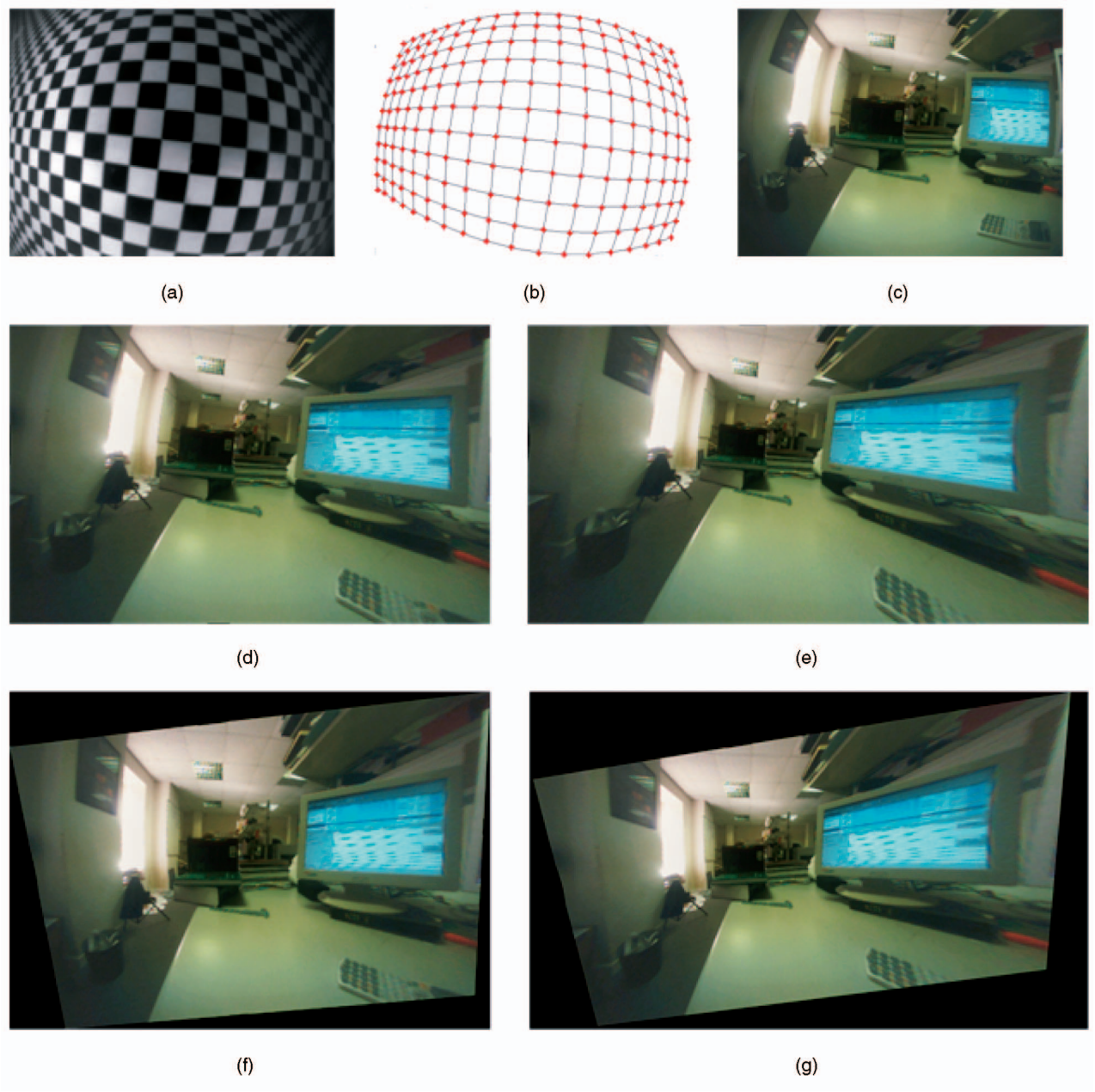

Fig. 10. Further rectification examples. (a) Checkerboard calibration diagram aligned with the rear wall of the room, (b) the extracted edges and corners, (c) original image, (d) using parameters from the circle fitting, and (e) conic fitting, (f) rectified using parameters from the circle fitting, and (g) conic fitting.

the ground truth data are unknown, the synthetic image results suggest that the result from the conic fitting is closer to the actual equidistance parameter of the camera. This is supported by the fact that the distribution of the estimations using conic fitting, tends to be smaller than the estimations using circle fitting. The results for the optical center estimation are similar for both cases, with the circle fitting again showing a slightly larger distribution than the conic fitting. These statements are supported by the data in Table 2, which shows the means and standard deviation of the sample real images for each camera. Note that Table 2 gives absolute averages and standard deviations for the parameters of the real cameras in contrast to Table 1, which gives averages and standard deviations for the errors in the parameter estimation.

The orientation parameter estimation errors are more difficult to quantify for the real images. The intrinsic parameters remain constant for each camera over the 15 images, while the extrinsic parameters, being the orientation of the camera against the checkerboard test diagram, will be different for each image due to the manual set up of the calibration rig. Table 3 shows the results for the orientation estimation for each of the 15 images from one of the cameras. The results for both the circle and the conic fitting methods are similar (never more than 0.5 of a degree in the difference), which suggests that the error in using either method will be similar. Additionally, the results from the synthetic images suggest that this error will be small.

Fig. 9 shows a checkerboard image from Camera 3, transformed to the rectilinear image using (11) with a back mapping method [21] and bilinear interpolation. Rotation is removed using the parameters from both circle and conic fitting methods, using the determined rotation matrix $\mathbf{R}$ and also using back mapping. It can be seen that using the parameters obtained from the conic fitting method returns an image with a greater degree of rectilinearity. This supports the results from the synthetic images that the estimation of f is more accurate using conic fitting. Fig. 10 shows further examples from Camera 2.

5 Conclusions

In this paper, we have demonstrated a method for extracting all the camera information required to provide a rectilinear, rectified image from a fish-eye camera. We have presented two methods: circle fitting and conic fitting. While the fitting of circles is undoubtedly a simpler method than fitting the general conic section equation to the project lines, we have shown that the fitting of conics returns better results, particularly in the equidistance parameter estimation.

The estimation of the optical center is a necessity. Hartley and Kang stated that (in a 640×480 image) the optical center can be as much as 30 pixels from the image center [4]. However, we have shown here that it can be greater than that with some consumer cameras. Our results from Camera 1 show a optical center that is almost 50 pixels from the image center, and Camera 2 is over 40 pixels. These deviations are significant, and should not be ignored in fish-eye camera calibration. In our tests on real images using moderate wide-angle to fish-eye cameras, the optical center estimation appears to be at least as good as the results presented by Hartley and Kang [4]. However, Hartley and Kang use averaging to reduce the effect of noise in their optical center estimations, which we have found is not necessary for our method. The estimation results of f, particularly for the conic fitting method, also show a low distribution.

Future work in the area would involve the examination of similar perspective properties for other lens models, as well as the examination of the effect of radial distortion parameters for fish-eye lenses that do not follow a particular model accurately.

Acknowledgments

This research was cofunded by Enterprise Ireland and Valeo Vision Systems (formerly Connaught Electronics Ltd.) under the Enterprise Ireland Innovation Partnerships Scheme.

References

[1] K. Miyamoto, "Fish Eye Lens," *J. Optical Soc. of Am.*, vol. 54, no. 8, pp. 1060-1061, Aug. 1964.
[2] *Manual of Photogrammetry*, C. Slama, ed., fourth ed. Am. Soc. of Photogrammetry, 1980.
[3] C. Hughes, R. McFeely, P. Denny, M. Glavin, and E. Jones, "Equidistant ($f\theta$) Fish-Eye Perspective with Application in Distortion Centre Estimation," *Image and Vision Computing*, vol. 28, no. 3, pp. 538-551, Mar. 2010.
[4] R. Hartley and S.B. Kang, "Parameter-Free Radial Distortion Correction with Center of Distortion Estimation," *IEEE Trans. Pattern Analysis and Machine Intelligence*, vol. 29, no. 8, pp. 1309-1321, Aug. 2007.
[5] S. Shah and J.K. Aggarwal, "Intrinsic Parameter Calibration Procedure for a (High-Distortion) Fish-Eye Lens Camera with Distortion Model and Accuracy Estimation," *Pattern Recognition*, vol. 29, no. 11, pp. 1775-1788, Nov. 1996.
[6] F. Devernay and O. Faugeras, "Straight Lines Have to Be Straight: Automatic Calibration and Removal of Distortion from Scenes of Structured Environments," *Int'l J. Machine Vision and Applications*, vol. 13, no. 1, p. 1424, Aug. 2001.
[7] L.L. Wang and W.-H. Tsai, "Camera Calibration by Vanishing Lines for 3-D Computer Vision," *IEEE Trans. Pattern Analysis and Machine Intelligence*, vol. 13, no. 4, pp. 370-376, Apr. 1991.
[8] B. Caprile and V. Torre, "Using Vanishing Points for Camera Calibration," *Int'l J. Computer Vision*, vol. 4, no. 2, pp. 127-139, Mar. 1990.
[9] N. Avinash and S. Murali, "Perspective Geometry Based Single Image Camera Calibration," *J. Math. Imaging and Vision*, vol. 30, no. 3, pp. 221-230, Mar. 2008.
[10] G. Wang, J. Wua, and Z. Jia, "Single View Based Pose Estimation from Circle or Parallel Lines," *Pattern Recognition Letters*, vol. 29, no. 7, pp. 977-985, May 2008.
[11] Y. Wu, Y. Li, and Z. Hu, "Detecting and Handling Unreliable Points for Camera Parameter Estimation," *Int'l J. Computer Vision*, vol. 79, no. 2, pp. 209-223, Aug. 2008.
[12] R. Strand and E. Hayman, "Correcting Radial Distortion by Circle Fitting," *Proc. British Machine Vision Conf.*, Sept. 2005.
[13] J.P. Barreto and K. Daniilidis, "Fundamental Matrix for Cameras with Radial Distortion," *Proc. IEEE Int'l Conf. Computer Vision*, vol. 1, pp. 625-632, Oct. 2005.
[14] C. Bräuer-Burchardt and K. Voss, "A New Algorithm to Correct Fish-Eye- and Strong Wide-Angle-Lens-Distortion from Single Images," *Proc. Int'l Conf. Image Processing*, vol. 1, pp. 225-228, Oct. 2001.
[15] B. Jähne, *Digital Image Processing*, fifth ed., ch. 12. Springer-Verlag, 2002.
[16] Z. Wang, W. Wu, X. Xu, and D. Xue, "Recognition and Location of the Internal Corners of Planar Checkerboard Calibration Pattern Image," *Applied Math. and Computation*, vol. 185, no. 2, pp. 894-906, Feb. 2007.
[17] F. Schaffalitzky and A. Zisserman, "Planar Grouping for Automatic Detection of Vanishing Lines and Points," *Image and Vision Computing*, vol. 18, no. 9, pp. 647-658, June 2000.
[18] Z. Zhang, "Parameter Estimation Techniques: A Tutorial with Application to Conic Fitting," *Image and Vision Computing*, vol. 15, no. 1, pp. 59-76, Jan. 1997.
[19] J.P. Barreto and H. Araujo, "Fitting Conics to Paracatadioptric Projections of Lines," *Computer Vision and Image Understanding*, vol. 101, no. 3, pp. 151-165, Mar. 2006.
[20] A.C. Gallagher, "Using Vanishing Points to Correct Camera Rotation in Images," *Proc. Second Canadian Conf. Computer and Robot Vision*, May 2005.
[21] K.V. Asari, "Design of an Efficient VLSI Architecture for Non-Linear Spatial Warping of Wide-Angle Camera Images," *J. Systems Architecture*, vol. 50, no. 12, pp. 743-755, Dec. 2004.